BeBeC-2022-D07

DE-REVERBERATION AND BACKGROUND NOISE REDUCTION TECHNIQUES FOR IMPROVING BEAMFORMING MAPS OF ENGINEERING NOISE SOURCES

Rohit Singh and Akhilesh Mimani
Department of Mechanical Engineering, Indian Institute of Technology Kanpur
Kanpur 208016, Uttar Pradesh, India

ABSTRACT

This paper presents an application of a de-reverberation technique along with a background noise reduction (BNR) algorithm for improving the beamforming maps used in imaging engineering noise sources located in a semi-reverberant environment. The de-reverberation technique is based on filtering the direct component of the cross-correlation matrix of the microphone signals recorded on an array, and is applicable in a general case. On the other hand, the BNR algorithm subtracts the background spectrum from the overall spectrum of the noise source(s). The method is demonstrated on different engineering applications which include a loudspeaker source located in a large hard-wall tunnel, a home appliance such as a mixer-grinder and a vertical drilling machine-tool. The results indicate that the cross-spectral conventional beamforming (CB) in a semi-reverberant environment fails to deliver an accurate prediction of the source location, especially with an increase in frequency. The implementation of the de-reverberation technique, however, is shown to significantly improve the localization accuracy which makes the source maps readily interpretable while in the case of machine-tool application, the BNR technique produces only marginal changes in the source maps.

1. Introduction

Acoustic cameras have nowadays become a standard tool for visualizing noise sources emitted from engineering applications and machinery [1-3]. A few applications of the acoustic camera include imaging noise sources generated from wind-turbines [4, 5], vehicle pass-by noise [6], aerospace structures in a wind-tunnel [7] and power-tools [8]. The hardware components of the imaging system essentially include a microphone array located at a certain distance from the source, a large channel-count data acquisition system (DAQ), a camera. The software records the sound data which is then usually used in a beamforming algorithm to compute an acoustic image that shows the hot-spots (focal-spots) representing the dominant noise sources. The acoustic image is then overlaid on the camera image wherein one can readily observe the location of noise source(s) in relation with the engineering application under consideration.

The underlying principle of a beamforming algorithm is to delay-and-sum the microphone signals with respect to different points in the scanning grid where the source location (usually assumed to be a monopole) is sought [9]. When the delay-and-sum beamforming (DSB) is implemented in the frequency-domain, it is termed as cross-spectral conventional beamforming (CB) in which the diagonal terms which represent the microphone self-noise are set to zero [10]. One of the main limitations of CB algorithms, however, is that it assumes a free-field propagation, i.e., it uses free-space Green's function of a monopole source to compute the steering vectors. This approach is less suited in reverberant/semi-reverberant environments which usually has multiple reflecting and scattering surfaces – the use of CB in such spaces often results in large side-lobes which completely mask the main lobe, i.e., the source making it difficult to identify the same in the map.

Several investigations have attempted to overcome the problems caused by reflection(s) – for instance, Guidati *et al*. [11] was the first one to propose the method of images to model reflections due to the wind-tunnel walls in a beamforming algorithm. Their results show that by incorporating reflections, one was able to better resolve airfoil trailing-edge noise sources using CB. The image source model (ISM) was also used by Fenech *et al*. [12], and more recently by Fischer and Doolan [13] to model reflections for localizing acoustic sources in a hard-wall tunnel using CB. The latter included a comparison of the ISM method with empirical de-reverberation algorithm based on steering vectors computed using numerical and experimental Green's function wherein it was found that the best resolution of the main lobe is obtained with the use of the experimental steering vectors. A few other representative works include the paper by Sijtsma and Holthusen [14] where reflections were modeled by taking into account the influence of a mirror source which is coherent with the main peak, the cepstral method proposed by Blacodon *et al*. [15] which removes the echoes by assuming that its quefrencies affect microphones differently but those of the source does not as well as the paper by Bousabaa *et al*. [16] which uses a computational aeroacoustics algorithm to numerically compute the Green's function for localizing sources in complex configurations such as a speaker located behind a diffracting sphere or on one side of a NACA0012 airfoil.

Fischer and Doolan [17] presented an interesting approach based on filtering the cross-correlation matrix (CCM) obtained from the cross-spectrum matrix (CSM) of the microphone array signals. In essence, they identified the mirror source(s) by means of different time-delays, i.e., the reflections observed in the CCM signals, and their effect was removed by multiplying each CCM vector by a window function centered at the main peak which corresponds to the direct source. The distinctive feature of their algorithm is that it is not geometry specific, in other words, the method is sufficiently general to be applied to de-reverberate the CSM for beamforming in a semi-reverberant or reverberant environment. The authors considered the test-cases of a loudspeaker source and a prototype NACA0012 airfoil located in a reverberant wind-tunnel test-section to demonstrate their method. The results show that de-reverberation was able to effectively suppress the side-lobes and reveal the actual source location. While the method is general for sure, it has not yet been used to improve the beamforming maps of real-time engineering noise sources which are located in a semi-reverberant environment without acoustic treatments. The objective of this work is therefore, to demonstrate the necessity and effectiveness of the de-reverberation algorithm on noise sources generated by engineering applications – the test-cases of a mixer-grinder home-appliance and a vertical drilling machine tool located in a semi-reverberant environment are considered here. Furthermore, for the machine-tool, the acoustic signature when the drilling machine is idling (no load) is referred to as background noise. In this work, we also consider the effect of implementing a background noise reduction (BNR) algorithm [18] on beamforming maps of noise sources generated when the drilling machine is under machining-load.

After briefly describing the beamforming algorithms, the paper takes up increasingly complex cases; we begin with the test-case of a loudspeaker in an anechoic and reverberant environments followed by the mixer-grinder test-case and finally, the vertical drilling machine.

2. Methodology: Beamforming algorithms

2.1 Cross-spectral Conventional Beamforming

This section briefly presents the equations describing the cross-spectral conventional beamforming (CB) algorithm for spatial location of acoustic sources in a free-space by making use of acoustic data recorded on a microphone array [7]. The microphone array measures acoustic pressure data at the microphone locations denoted by $\mathbf{X}_m$ and the acoustic data is stored in a n-dimensional acoustic pressure vector corresponding to n microphones given by

$$\mathbf{p} = \{p_1(f) \quad p_2(f) \quad \cdots \quad p_n(f)\}^T , \tag{1}$$

where f denotes the frequency (Hz). The source strength at a generic point $\boldsymbol{\xi}_S$ in the scanning plane can be expressed as

$$\mathbf{p} = a\mathbf{g}(\mathbf{X}_m - \boldsymbol{\xi}_S), \tag{2}$$

where $\mathbf{g} = \dfrac{e^{-jk_0\mathbf{r}}}{4\pi\mathbf{r}}$ denotes the free-space Green's function vector also known as the steering-vector, $\mathbf{r} = |\overrightarrow{X_m} - \overrightarrow{\xi_s}|$ and k_0 = wavenumber. In order to determine the complex amplitude a at the assumed source location in the scanning grid, we minimize the least-squares equation

$$E = \|\mathbf{p} - ag\|^2 , \tag{3}$$

to obtain the complex amplitude $$a = \frac{g^H\mathbf{p}}{\|g\|^2} \tag{4}$$

The beamforming output $B(\mathbf{X}_m, f)$ over the scanning plane is then given by

$$B(\mathbf{X}_m, f) = \frac{\mathbf{g}^H\mathbf{C}\mathbf{g}}{\|\mathbf{g}\|^4} \tag{5}$$

where $\mathbf{C} = \overline{\mathbf{p}(f)\mathbf{p}(f)^H}$ denotes the cross-spectral matrix (CSM), the superscript denotes the Hermitian transpose while the superscript $\overline{X}$ denotes the averaging of the quantity X in a number of discrete time blocks using Welch's periodogram. The diagonal terms of the $\mathbf{C}$ matrix pertain to the auto-spectra or the microphone self-noise; it does not contain phase information required for beamforming, and thus, it is set to zero. The source location corresponds to the maximum of the beamforming output in the scanning plane.

2.2 De-reverberation: Filtering the cross-correlation matrix (CCM)

This section briefly describes the de-reverberation algorithm originally proposed in Fischer and Doolan [17]. We consider the case of a single microphone in a reverberant environment where the reflections can be seen in the auto-correlation function of the microphone that is similar to auto-spectrum in the frequency-domain. The time-domain cross-correlation function can be defined for signal $x(t)$ and time length T as follows.

$$C_{xx}(\tau) = E[x(t)x(t+\tau)] = \frac{1}{T}\int_0^T x(t)x(t+\tau)\,dt \tag{6}$$

The function will exhibit a peak at $\tau = 0$ because there is no delay when the signal is equal to itself. However, in a reverberant environment, a second peak will appear after some time delay between the direct and reflected sound. Similarly, the cross-correlation function between two signals can be written as

$$C_{xy}(\tau) = E[x(t)y(t+\tau)] = \frac{1}{T}\int_0^T x(t)y(t+\tau)\,dt. \tag{7}$$

For two discrete signals of the same length N, the cross-correlation function is given by

$$C_{xy}(q) = \frac{1}{P}\sum_{p=1}^{P} x(p)y(p+q) \tag{8}$$

While the time-delay τ can be obtained experimentally by placing a loudspeaker source in the reverberant test-section, in this work, the cross-correlation function is determined by taking inverse fast Fourier transform (*ifft*) of the cross-spectrum function. After computing the cross-correlation, one needs to process the data to remove reflections in the time-domain. To this end, each time-vector in the cross-correlation function is multiplied with a Hanning window function centered at the main lobe implying that only the direct field is retained while the remaining signals contaminated with reflections and scattering of the source are over-written with zeros.

The width of the window should be optimized in order to ensure that it is large enough to retain sufficient information about the main lobe but small enough to remove the reflections. Indeed, optimization of the filtering window length is carried out through a trial-and-error procedure which aims at achieving the best possible source resolution and minimum localization error. For the different test-cases considered here, we first present the cross-correlation graphs which shows the direct field (peak at t = 0) and multiple reflected fields; the optimized filtering window is indicated by a box in the graphs while the number of optimized data points is noted in the text. This filtering process is applied to all the time-vectors in the cross-correlation matrix to obtain the filtered cross-correlation matrix (FCCM). Finally, to compute the frequency-domain filtered cross-spectrum matrix (FCSM), fast Fourier transform (*fft*) is applied to FCCM components. The FCCM is then used in the conventional beamforming algorithm; the maps obtained by this de-reverberation procedure are henceforth referred to as de-reverberation maps (DBF).

2.3 Background Noise Reduction (BNR)

The background noise reduction (BNR) which is one of the most popular denoising method [18] is briefly described. This method assumes that the measured signal can be decomposed into two *uncorrelated* components, namely, the source and the background noise. In terms of CSM, this can be written as

$$\mathbf{C} = \mathbf{C}_s + \mathbf{C}_d \tag{9}$$

Here, **C** is obtained by experimentally and contains acoustic data pertaining to the noise source which needs to be imaged as well as the noise produced by background process. On the other hand, $\mathbf{C}_d$ pertains to the CSM when only the background process is taking place. The denoising is implemented by subtracting $\mathbf{C}_d$ from **C**, thereby yielding **C**s or the CSM of the actual noise source only which is used in the beamforming algorithm.

Note that when background noise needs to be filtered, we first implement the BNR algorithm followed by de-reverberation method described in section 2.2.

3. Experimental set-up and beamforming results

The efficiency of de-reverberation and BNR algorithms for improving beamforming maps is assessed on noise sources generated by different engineering applications. In this section, the test-cases are considered in an increasing order of complexity; for each test-case, we briefly describe the experimental set-up before proceeding to discuss the results, i.e., the source maps.

3.1 Acoustic instrumentation and data acquisition system

The microphone array comprises of 32 G.R.A.S. 40PH ¼" microphones arranged in an Underbrink spiral array design which delivers an optimal overall performance at low and high frequencies. To determine the spatial locations of the microphones in the Underbrink design, one requires the minimum and maximum radii along with the spiral angle which were set to r_0 = 50 mm, r_m = 500 mm and $\nu = 5\pi/16$, respectively, for details, refer to Prime and Doolan [19]. Further note that one microphone was placed at the origin (0, 0, 0) which ensures a satisfactory performance in the low-frequency range. The microphones were connected through BNC cables to 4497 PXIe National Instruments (NI) data acquisition (DAQ) cards which are mounted on a 1073 NI PXIe chassis. The DAQ system was connected to a high-performance desktop with i7, 11th generation processor and 32 GB RAM while the signals are acquired through a LabView program. The microphone array and DAQ system is portable, and is used to record noise data for different test-cases considered in this investigation at a sampling frequency $f_s = 65536$ Hz $(\Delta t = 1.5259 \times 10^{-5}$ s$)$ and sample time T = 10 s.

3.2. A loudspeaker noise source

First, the efficiency of the de-reverberation algorithm is demonstrated on a loudspeaker source in a hard-wall large wind-tunnel and the results are compared with those obtained in an anechoic environment.

Figure 1(a) shows a SONY SRS-XB12 loudspeaker source (46 mm diameter and effective operating frequency range from 100 Hz to 7000 Hz) placed in front of the spiral microphone array, and the set-up is placed in an anechoic chamber which is made of high-quality polyurethane (PU) foam wedges with working dimensions, i.e., tip-to-tip distance is 5 m x 5 m x 3 m. The chamber cut-off frequency is 200 Hz, i.e., it provides a reflection-free environment above this frequency, and the noise rejection ratio with respect to the outside environment is 65 dB(A). The perpendicular distance between the spiral array plane and the source was fixed at 1.5 m with the center microphone of the array taken as the origin (0, 0, 0). Note that with respect to these co-ordinates, the center of the speaker is located at (0, 0, 1.5 m). On the other hand, Fig. 1(b) shows the same loudspeaker mounted on a wooden stand located at the center of the test-section of the National Wind Tunnel Facility (NWTF) which is a closed-circuit, wind-tunnel having a closed test-section of height 2.25 m, width 3 m and length 8.75 m. Here, two glass windows of the NWTF test-section were replaced by a thick plywood in which holes were drilled to arrange microphones at different locations pertaining to a slightly modified Underbrink spiral. The modification was necessary due to the presence of a 150 mm thick metal strip between the glass walls where holes cannot be drilled, therefore, the microphones whose original location belongs to the strip region needs to be shifted further down by the said distance.

The acoustic data from the speaker was recorded for the case of no flow (stationary medium), i.e., the tunnel was not operated, rather, the objective here is to check the efficiency of the de-reverberation technique in a highly reverberant environment of the NWTF test-section. The loudspeaker is made to emit tonal noise at $f_0 = \{500, 1000, 2000, 4000\}$ Hz which corresponds to the center frequencies of one-third octave bands.

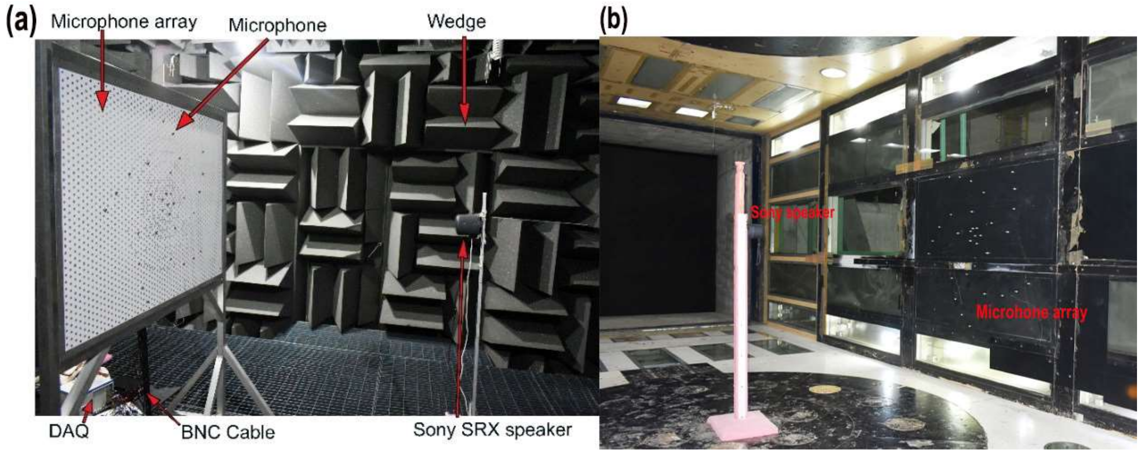

Figure 1 The photograph shows a loudspeaker speaker (a) in an anechoic chamber and (b) in the test-section of the National Wind Tunnel Facility (NWTF) at IIT Kanpur.

Figures 2(a-d) present the source maps computed using the CB algorithm in the anechoic chamber at the tonal frequencies (in that order) indicated above. Note that the maps are normalized with respect to the strength of the focal spot, i.e., the source strength, and the results are shown over a dynamic range [0, -15 dB]. The same convention is followed for the remaining source maps presented in this work. As anticipated, the CB method works well in the anechoic chamber for a loudspeaker – the circular focal spot represents the source wherein it is observed that predicted location (focal point) denoted by a cross X is co-incident with the known location indicated by a circle O which is taken at the center of the circular cross-section of the loudspeaker. Furthermore, the resolution increases, i.e., focal spot size decreases with increase in frequency.

Figures 2(e-h) presents the CB source maps of the loudspeaker located in the NWTF test-section at the same tonal frequencies noted above while Figs. 2(i-l) show the counterpart DBF maps. It can be readily noted that in the highly reverberant NWTF test-section, the CB method produces an error in source localization which is more evident at low frequencies, refer to Table 1. Furthermore, reflections due to the hard walls of the tunnel produce side-lobes which make it somewhat difficult in identifying the focal spot that represents the source. The occurrence of reflections can be readily appreciated from Fig. 3 which shows the auto-correlation graph for the center microphone for the 1000 Hz signals in the NWTF test-section. We observe a peak due to first reflection at t = 2.57 ms, i.e., 169 data points which gives the time beyond which the signals will be contaminated with reflections. However, considering the auto-correlation graphs of all 32 microphones, it was found that the maximum window which accounts *only* for the direct field is 0.98 ms, i.e., 64 data points which is shown by a black box in Fig. 3. Now, in order to determine the optimal direct field window, the evolution of source localization error and resolution as a function of half-window L_{hw} was studied for all frequencies ranging from 500 Hz to 4000 Hz, and it was found that $L_{\mathrm{hw}} = 5$ data points delivers an optimal trade-off in localization error and resolution. Therefore, the full-window $L_w = 2L_{hw} + 1 = 11$ data points were considered while computing the DBF source maps. Figures 2(i-l) show that when the de-reverberation technique is applied, the localization error is significantly reduced (see Table 1) whilst the resolution also improves noticeably, although the resolution is still poor at low frequencies. Note that at higher frequencies 4000 Hz and beyond, the improvement in localization accuracy and resolution is marginal. Nevertheless, these results do highlight the utility of the de-reverberation technique and in fact, encourage its implementation to more challenging engineering applications.

Table 1 Error in localization normalized with respect to the wavelength λ_0 for different algorithms in anechoic chamber and reverberant NWTF test-section.

Frequency f (Hz)	Non-dimensional localization error: Δ/λ_0		
	CB: Anechoic chamber	**CB: NWTF**	**DBF: NWTF**
500	0.04	0.64	0.05
1000	0.01	0.43	0.23
2000	0.23	0.34	0.23
4000	0.26	0.92	0.22

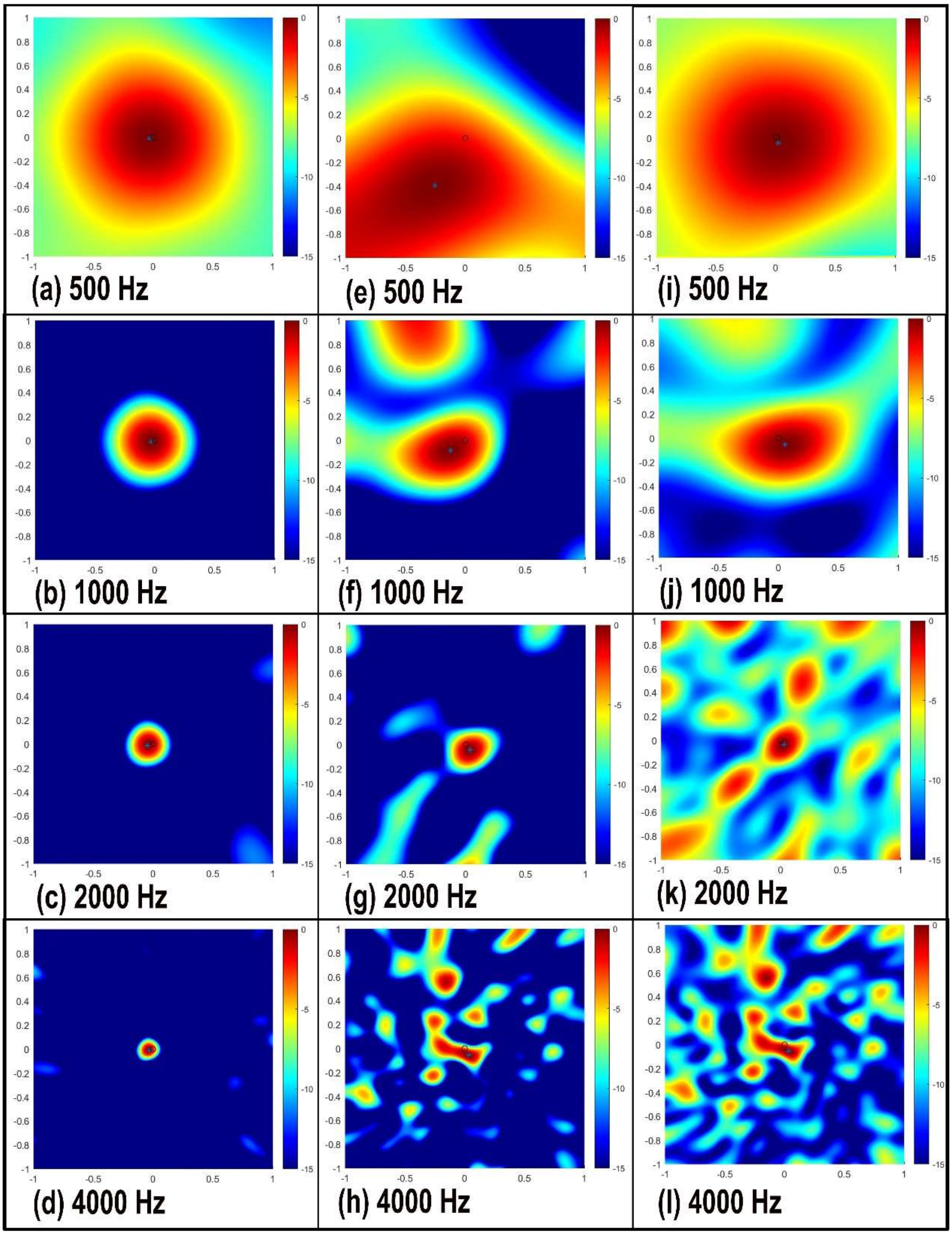

Figure 2 Parts (a-d) shows the CB source maps of a loudspeaker in an anechoic chamber while parts (e-h) show the CB maps of the same source in the reverberant NWTF test-section. Parts (i-l) are computed by implementing the de-reverberation algorithm on the acoustic data recorded in NWTF.

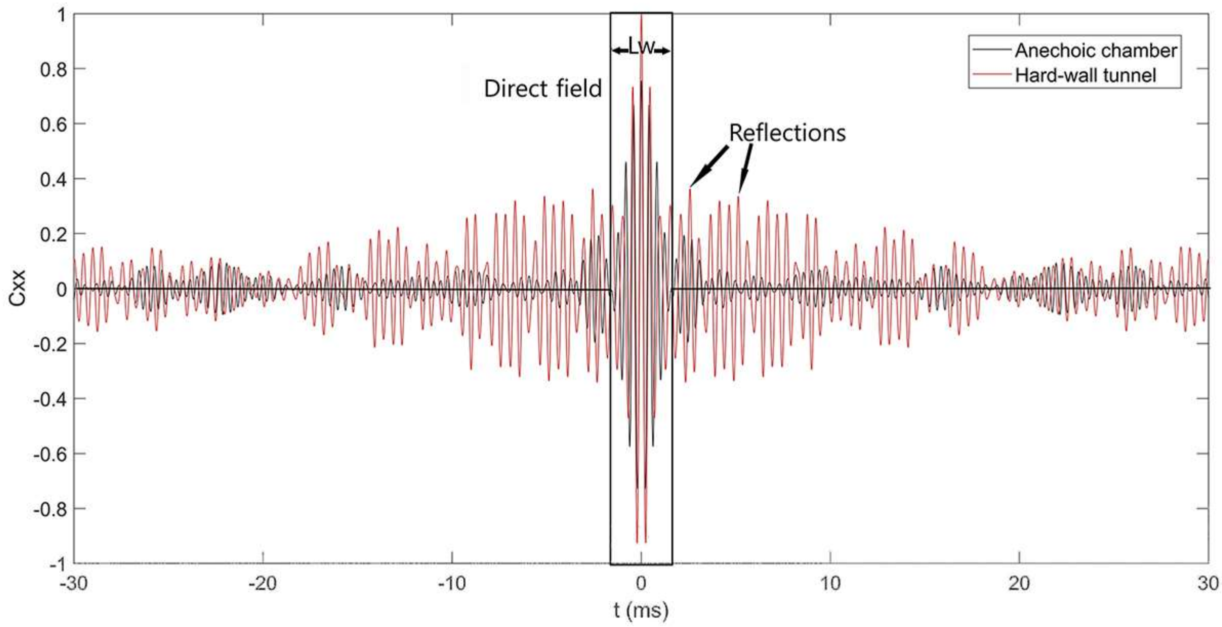

Figure 3 The auto-correlation functions pertaining to the center microphone of the spiral array for the loudspeaker source emitting tonal noise at 1000 Hz in the anechoic chamber and the reverberant NWTF test-section. For data obtained in the anechoic chamber, the auto-correlation graph does not show reflections, rather, the signals decay gradually.

3.3. Mixer-grinder home-appliance

Figures 4(a) and (b) show the photograph of a Bajaj GX 3701 mixer-grinder home appliance located in (a) anechoic chamber and (b) semi-reverberant office environment which has multiple hard scattering/reflecting surfaces. The power rating of the mixer-grinder is 750 Watt, and maximum speed of 18000 RPM with four blades meant for heavy-duty grinding. The acoustic data is measured by the Underbrink spiral array of microphones placed at a distance 1.5 m from the mixer-grinder.

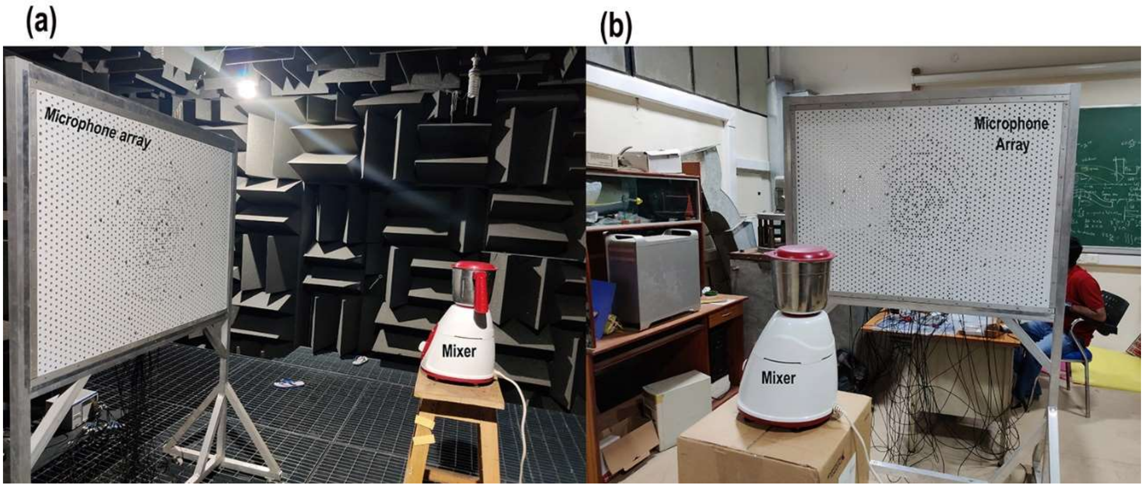

Figure 4 Photographs showing the experimental set-up of a mixer-grinder and spiral microphone array in (a) anechoic chamber and (b) semi-reverberant office space.

Figure 5 shows a comparison of the acoustic spectra measured at the center microphone of the mixer-grinder noise obtained in the anechoic chamber with that obtained in the semi-reverberant office space. Both spectra are observed to be similar, however, the one obtained in the semi-reverberant environment is significantly higher (approximately 13 dB) than its anechoic chamber counterpart as anticipated. Furthermore, the anechoic chamber spectrum has a much clear definition of multiple peaks which occur at exact integer multiples, e.g., note the peaks at 304 Hz, 608 Hz, 912 Hz, 1224 Hz and so on. The peak frequencies are most likely attributed to the noise at integer multiples of blade passing frequencies of the rotating blades within the grinder pot as well as motor noise. Additionally, the structural vibration of the mixer body also contributes to the far-field radiated noise.

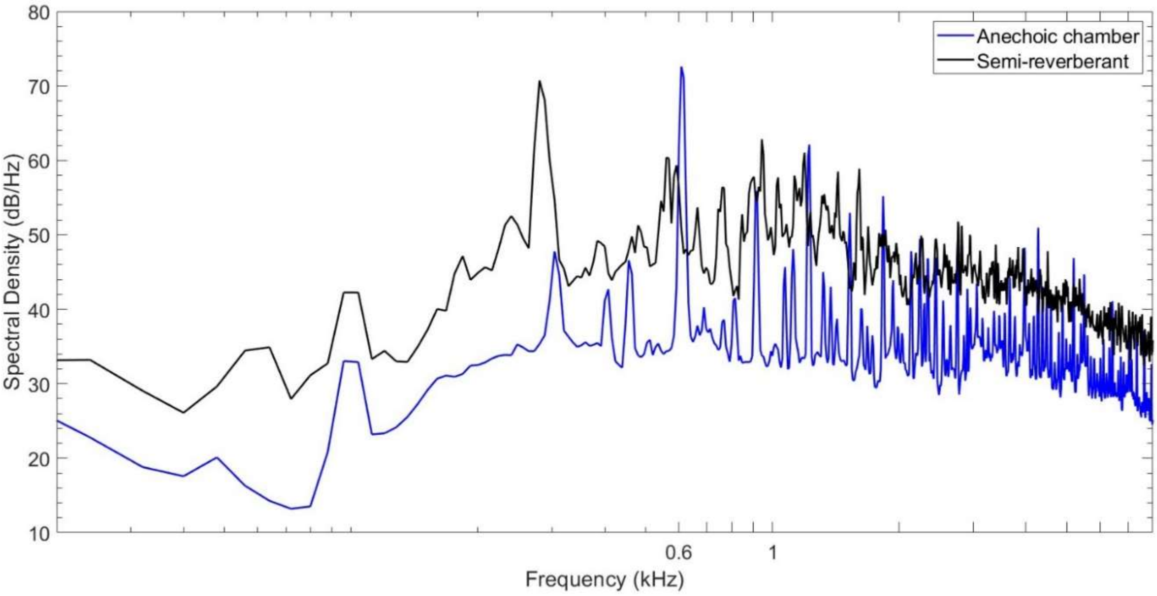

Figure 5 Comparison of the acoustic spectrum of the mixer-grinder in anechoic chamber, and in the semi-reverberant environment.

Figures 6(a-h) show the CB source maps spanning low-to-high frequencies for the data obtained in the anechoic chamber. Figure 6(a) shows that at 600 Hz, a rather poor source resolution is obtained although one can appreciate that the mixer-grinder is the noise source. (Note that at the first blade passing frequency equal to 304 Hz, the resolution is even worse, thus, the CB map is not shown at such low frequency.) However, at higher frequencies, the CB method completely fails as the focal spot, i.e., the predicted source is observed well-below the mixer-grinder which certainly indicates a large error. This seems to suggest that even in an anechoic environment, it is difficult for the microphone array to record only the direct field due to a significant scattering of waves by the mixer-grinder itself and also because of reflections by the array surfaces. Therefore, the CB method needs to be modified based on the de-reverberation technique even when an anechoic environment is used for testing real-time sources. To this end, Fig. 7 shows the auto-correlation graphs pertaining to the center microphone for the mixer-grinder in anechoic as well as the semi-reverberant office environment. For the anechoic environment, the graph does decays with time but it is characterized by the presence of multiple peaks due to reflections as annotated in the figure. Similar remarks also hold for the graph pertaining to the semi-reverberant office space, however, in this case, the reflected peaks are prominent and can be readily observed. For both cases, the first reflection peak occurs at 9.86 ms, however, considering all 32 microphones, the first reflection occurs at 1.63 ms, i.e., 107 data points in the half-window. The best possible resolution and localization accuracy was obtained when L_{hw} equals 51 data points, i.e., the rectangular window L_w contains 103 data points. In view of this discussion, it can be concluded that for determining the optimal direct field window for a given engineering noise source, a trial-and-error procedure needs to be followed.

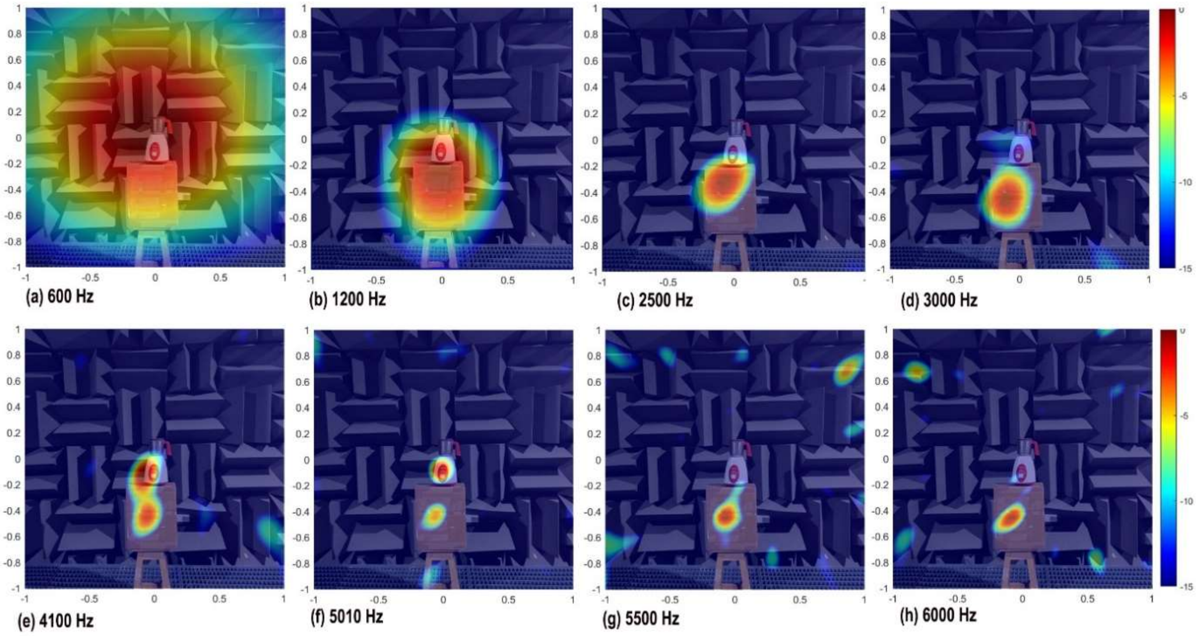

Figure 6 CB source maps of the mixer-grinder in the anechoic chamber in the frequency range from 600 Hz to 6000 Hz.

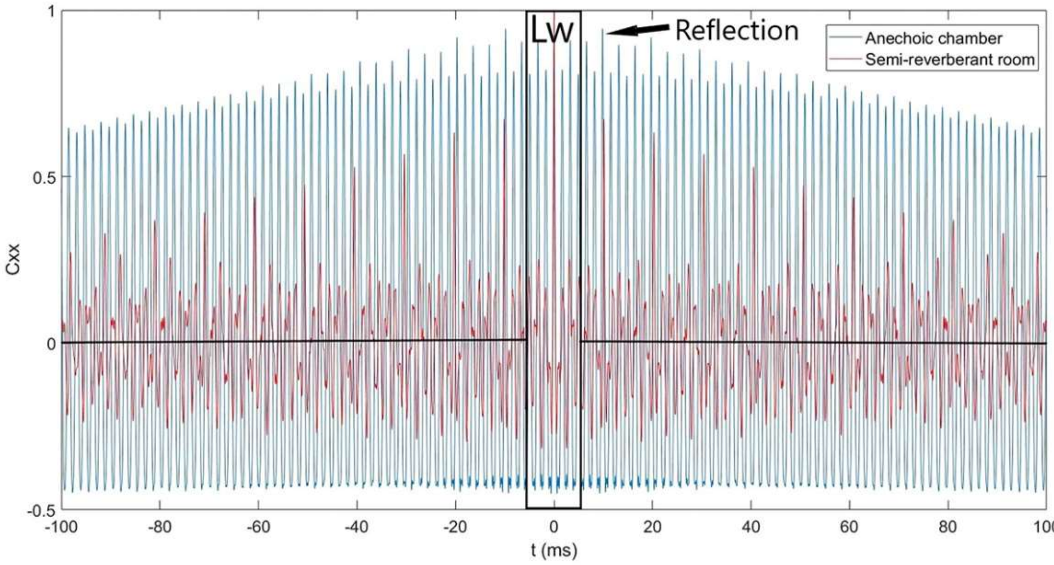

Figure 7 The auto-correlation functions for the mixer-grinder source in the anechoic chamber and semi-reverberant office space.

Figures 8(a-h) show the DBF maps at the same frequencies using the anechoic chamber data. While the resolution, especially at low frequencies is still poor, the de-reverberation dramatically improves the source localization accuracy – the focal spots are now observed right at the mixer. In fact, at higher frequencies 5010 Hz and beyond, one is able to readily note the source directivity as may be appreciated from the multiple lobes centered at the mixer-grinder.

Figures 9 and 10 show the CB and DBF maps using the data obtained in the semi-reverberant office environment. It is readily observed that the CB method fails completely from 1200 Hz onwards whereas the DBF method works reasonably well as it is easy to observe the source location at the mixer-grinder at all frequencies considered. However, a comparison of Figs. 7(a-h) with counterpart results shown in Fig. 9 shows that the anechoic chamber is far-better suited for the localization due to significantly reduced noise levels in the focal (source) spot vicinity in the former case. Nevertheless, the Figs. 6, 8 to 10 collectively demonstrate the efficiency and importance of the de-reverberation algorithm for localizing noise sources from a real-time engineering application.

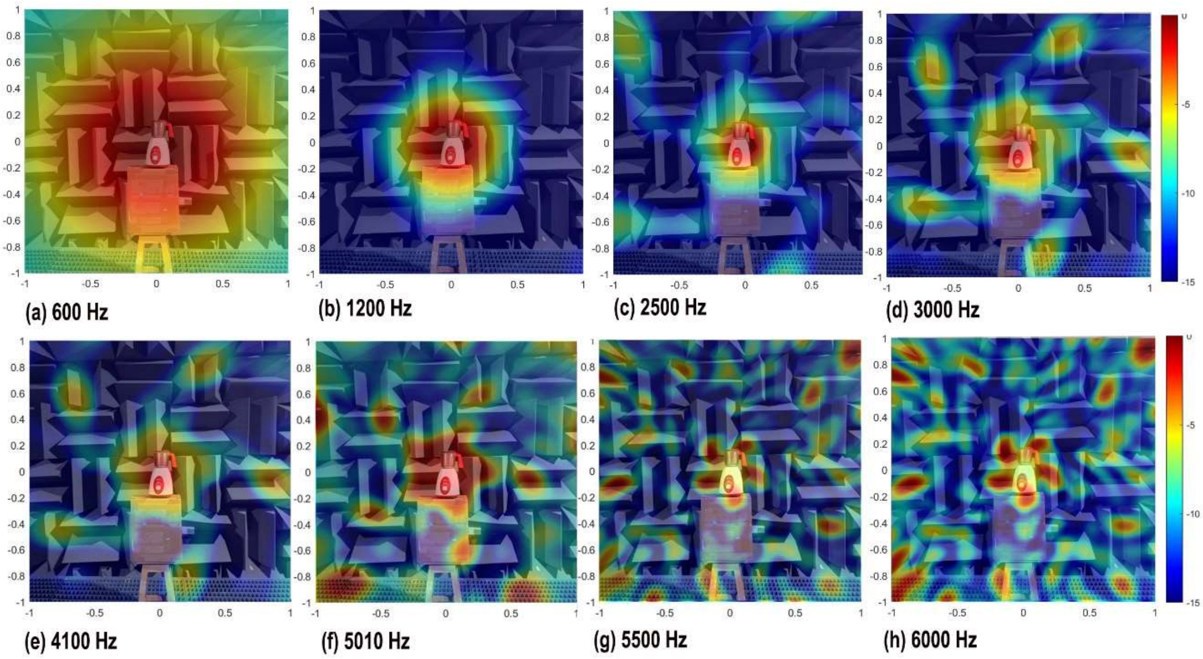

Figure 8 DBF source maps of the mixer-grinder in the anechoic chamber in the frequency range from 600 Hz to 6000 Hz.

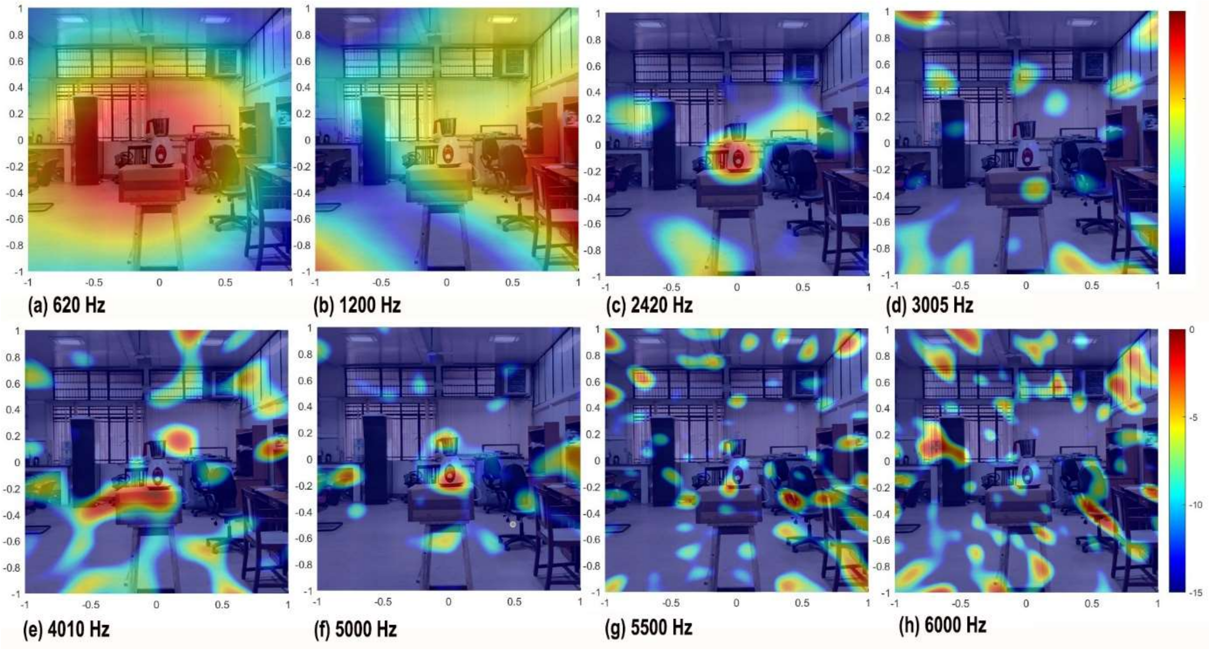

Figure 9 CB source maps of the mixer-grinder in the semi-reverberant office environment in the frequency range from 600 Hz to 6000 Hz.

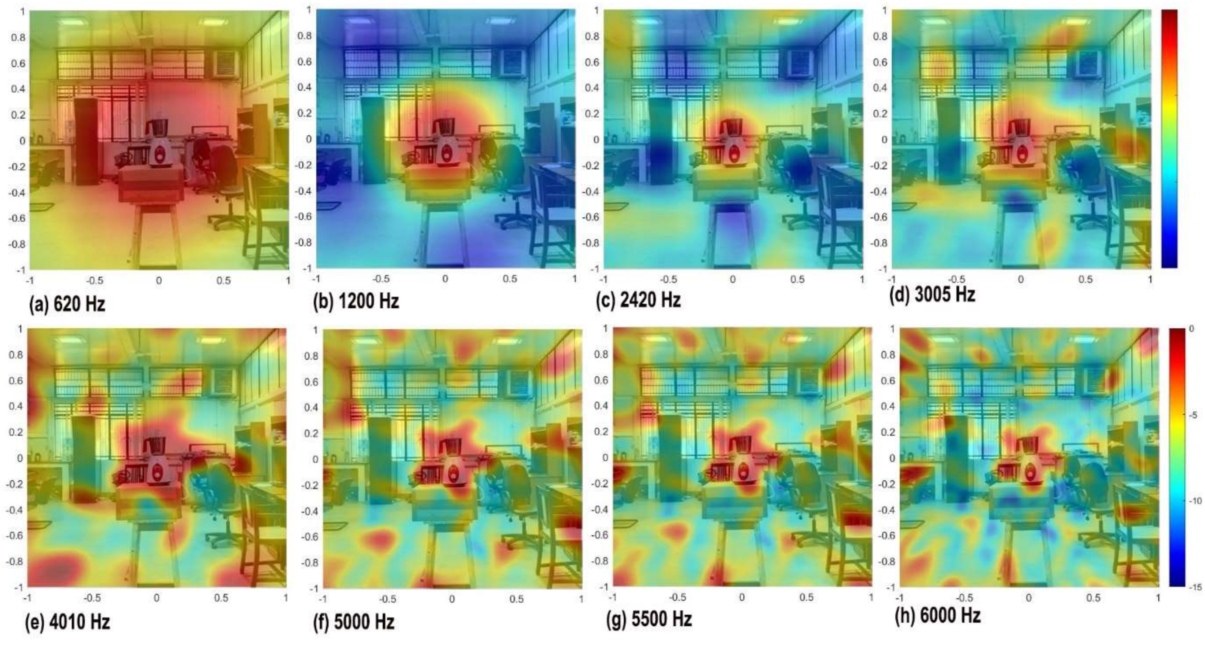

Figure 10 DBF source maps of the mixer-grinder in the semi-reverberant office environment in the frequency range from 600 Hz to 6000 Hz.

3.4. Vertical drilling machine-tool

Figure 11 shows a photograph of the vertical drilling machine located in a semi-reverberant environment of the workshop (Imagineering laboratory, IIT Kanpur) where different components of the drilling machine are annotated. The drilling machine has a 1.1 KW motor with approximate speed of 1900 rpm which is connected to the gearbox by the belt-drive to maintain a constant cutting speed at the tool-piece. A parallel twist-drill of 8 mm diameter is used to drill a mild steel specimen. The spiral array faces the drilling machine and is located at a distance of 1.5 m from it.

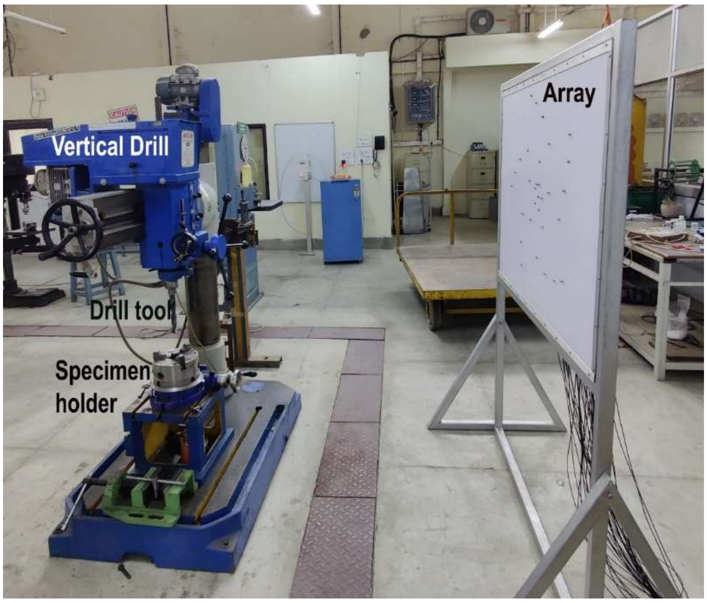

Figure 11 Photograph depicting the experimental set-up of a vertical drilling machine and spiral microphone array in the semi-reverberant workshop environment.

Figure 12 shows the acoustic spectra measured at the center microphone when the drilling operation was carried out, i.e., during machining-load conditions, and also when the drilling machine was running (idling) but the workpiece was absent, i.e., under no machining-load condition. Both spectra are comparable in the low-frequency range up to 280 Hz beyond which the spectrum pertaining to the drilling operation is significantly higher (18 dB) and in fact, runs nearly parallel to the case when the machine is running but drilling does not take place. Both spectra exhibit multiple peaks at nearly the same frequencies; the low-frequency broadband hump and peaks are due to the vibrations of the machine base and motor noise, respectively, while the higher frequency peaks are most likely attributed to the gear-box and other power-transmission components which possibly experiences a much higher mechanical load during the drilling operation. Additionally, the contact point of the drill-bit and specimen may also contribute to the radiated noise spectrum.

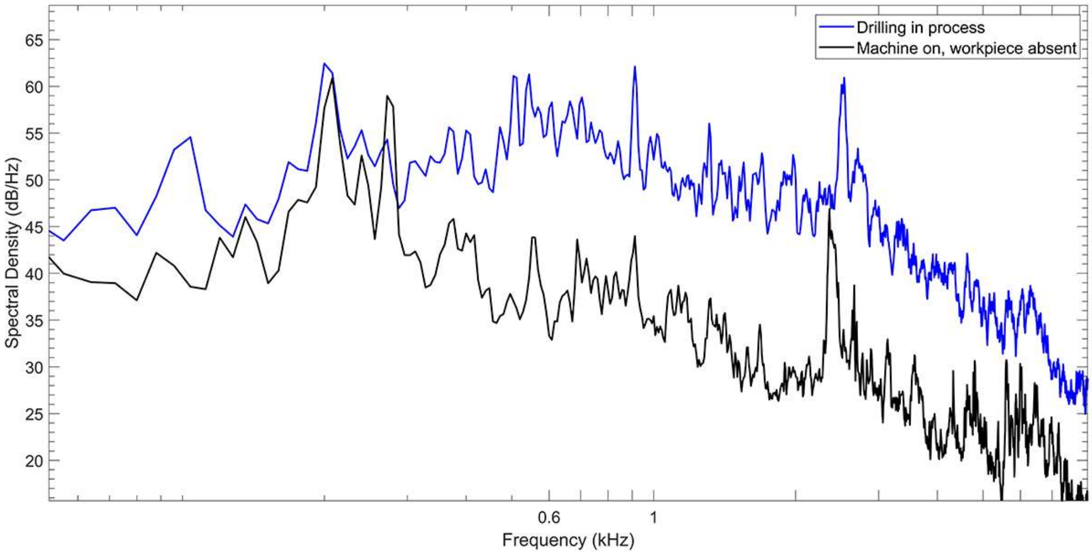

Figure 12 Acoustic spectrum of the mixer-grinder when drilling is carried out and when the machine is running but the workpiece is absent.

Figures 13(a-h) show the CB source maps spanning low-to-high frequencies pertaining to the drilling noise spectrum. Note that vertical drilling machine photograph is watermarked in the background which makes it easy to interpret the source distribution obtained. It is readily observed that at very low frequency f_0 = 200 Hz, the machine-base is the dominant noise source as anticipated while a significant error is observed in the source location at 800 Hz although both results suffer from a poor resolution. While the results at 1200 Hz and 2500 Hz suggest that the dominant noise sources reside at the gearbox and specimen holders, respectively, and therefore, are somewhat satisfactory, the CB maps at 3000 Hz and beyond fail to provide a meaningful result due to the observed location of the focal spots. To resolve this issue, we dereverberate the signals by separating out the direct field from the total (direct + reflected) field as illustrated in the auto-correlation graph shown in Fig. 14. Considering all microphones, the minimum time at which the first reflected peak occurs is 5.27 ms, i.e., 345 data points in half-window. However, following a trial-and-error procedure, the half-window size L_{hw} = 63 data points which ensures that the localization accuracy/resolution is satisfactory, and at the same time, one does not discard or lose too much direct field noise data.

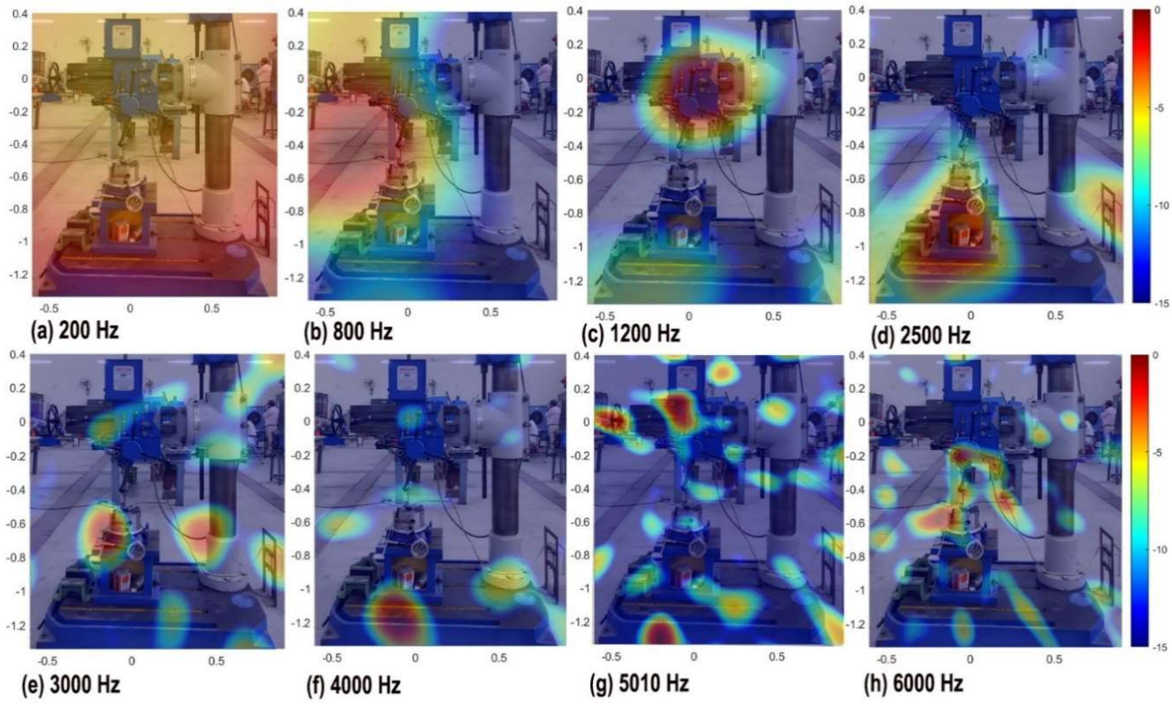

Figure 13 CB source maps for the vertical drilling machine in the semi-reverberant environment at the workshop in the frequency range from 200 Hz to 6000 Hz.

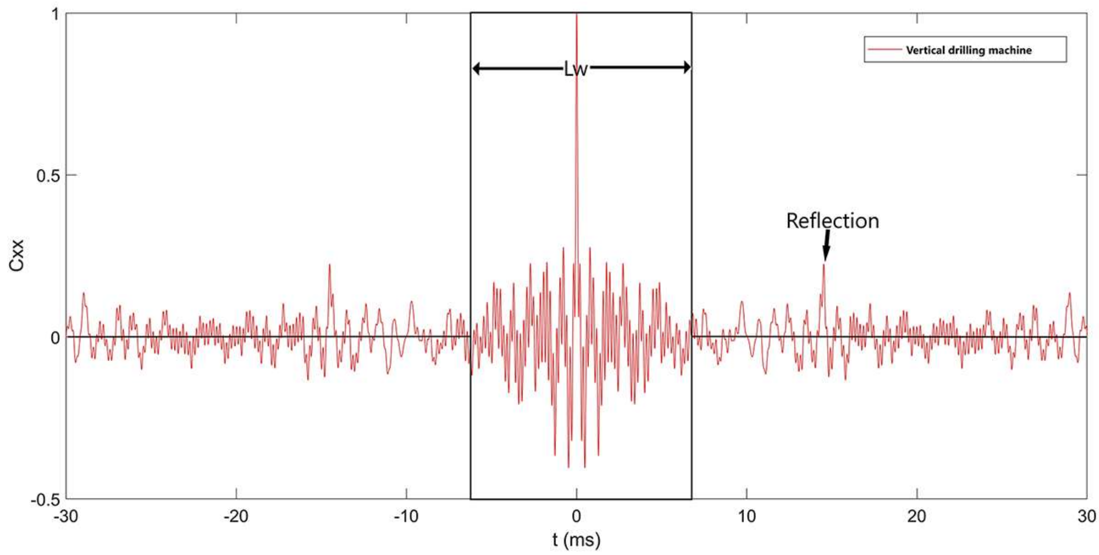

Figure 14 The auto-correlation function for the vertical drilling machine located in the reverberant environment in the workshop. The window pertaining to the direct field is shown by the box.

Figure 15 shows the DBF source maps while Fig. 16 shows the DBF + BNR source maps pertaining to the drilling noise spectrum at the same frequencies as presented in Fig. 13. The DBF source maps clearly show a noticeable improvement in the source location accuracy from 1200 Hz and beyond; by using only the direct field, the focal spots are now observed at the anticipated location(s). For instance, at 1200 Hz, the upper part of the machine which includes the gearbox is observed to be the dominant noise source while at 2500 Hz and 3000 Hz, the noise sources are apparently located in the lower part. However, note that noise is generated due to the contact of the drilling tool and specimen, and it may be possible that it is transmitted to the specimen holder, i.e., the lower region. Nonetheless, a poor resolution is observed, and it may be possible to obtain a more accurate estimation of the source location by implementing a deconvolution algorithm on this map. At this stage, it may be noted that the DBF maps at 2500 Hz and 3000 Hz were also computed with window size $L_w = 1$ data point, however, in this case, a much weaker noise source was observed only near the gear box region while the much stronger source at the lower regions observed in parts (d) and (e) was completely absent. This demonstrates one must carefully select the optimal window such that important direct field noise data is retained. The source map at 4000 Hz shows equal noise contributions be different components of the machine. At higher frequencies given by 5010 Hz and 6000 Hz, the dominant noise sources are again observed near the gear box and power transmission components. Furthermore, at 6000 Hz, the directivity of the source near the gearbox may be easily observed. Figures 16(a-h) are nearly identical with their counterpart maps shown in Figs. 15(a-h), however, a small improvement in focal-resolution is observed at 2500 Hz and 3000 Hz in the former case. This demonstrates that in this case, the background noise removal is not necessary because the acoustic spectrum when drilling was not carried out was significantly lower as discussed previously.

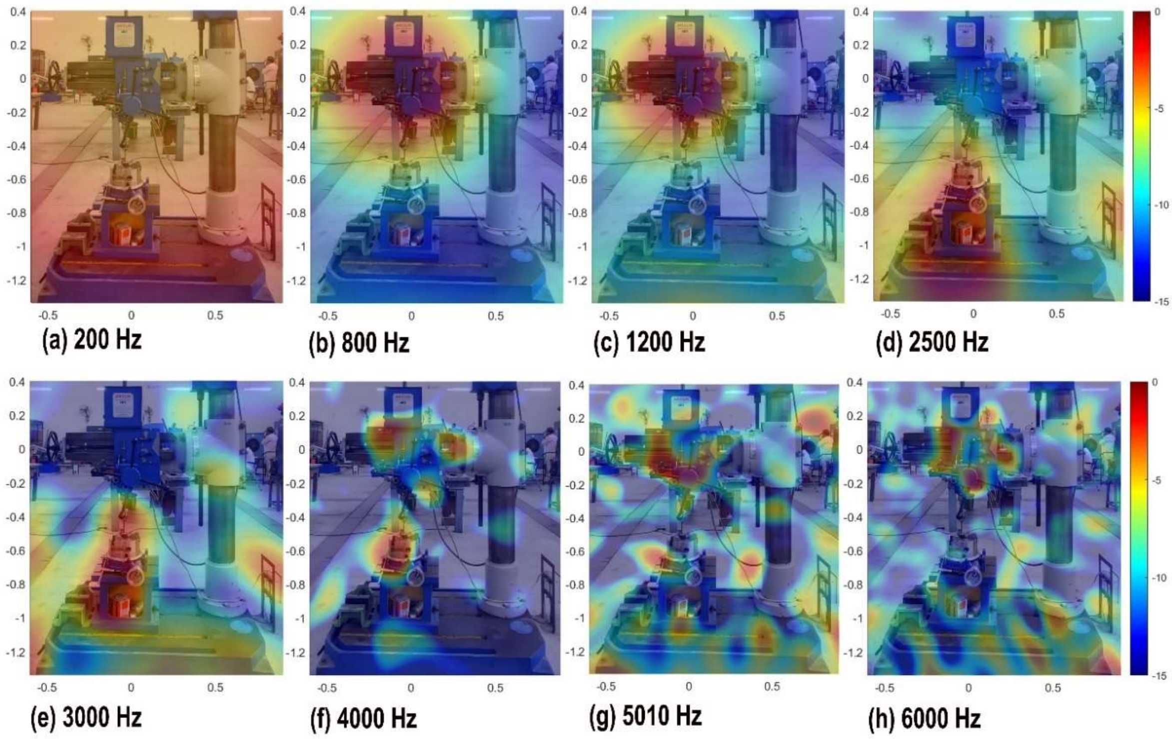

Figure 15 DBF source maps for the vertical drilling machine in the semi-reverberant environment at the workshop in the frequency range from 200 Hz to 6000 Hz.

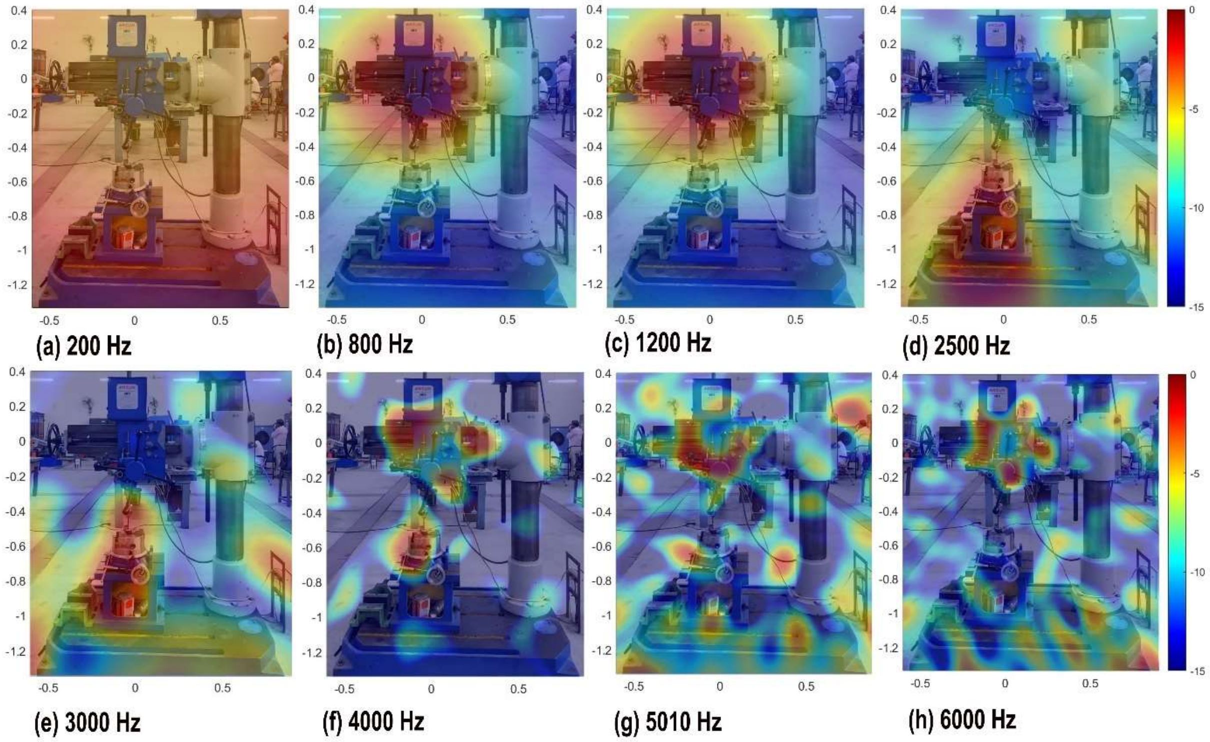

Figure 16 DBF + BNR source maps for the vertical drilling machine in the semi-reverberant environment at the workshop in the frequency range from 200 Hz to 6000 Hz.

4. Conclusions

This paper has demonstrated the application of a de-reverberation technique proposed by Fischer and Doolan [17] to improve the beamforming source maps of real-time engineering noise sources placed in a semi-reverberant environment. The results suggest that for an accurate localization of sound sources from an engineering application such as a mixer-grinder home appliance placed in an anechoic chamber during testing, the CB method fails at higher frequencies and it is necessary to de-reverberate the microphone signals. The DBF maps, on the other hand, not only deliver an accurate source localization but also reveal the source-directivity at higher frequencies. Similar conclusion was also arrived at for the mixer-grinder case in a semi-reverberant office environment. For the case of a vertical drilling machine-tool, the simultaneous application of de-reverberation and background noise reduction (BNR) method produces nearly the same results as those obtained by the application of only de-reverberation technique. This is most likely attributed to the fact that the acoustic spectrum levels are significantly higher when the drilling operation is carried out, i.e., when the workpiece is being machined in comparison to the background levels when the drilling machine is idling, i.e., under no machining-load. However, it is possible that in the case of other machine-tools for which the noise levels under machining-load and idling conditions are comparable, it may be necessary to implement BNR or other similar techniques to visualize the location and extent of noise source(s) which may be dominant near the work-toolpiece contact region. This will be a subject matter of a future investigation along with the implementation of deconvolution techniques such as CLEAN-SC [7] or DAMAS [20] on DBF + BNR maps which is likely to significantly enhance the resolution of machine-tool noise source(s).

Acknowledgments

This work was funded by the Science Education and Research Board (SERB) New Delhi, INDIA through its Start-up Research Grant SRG/2019/000885 '*Resolving airfoil self-noise mechanism using diagnostic acoustic imaging tool*' – the authors gratefully acknowledge the financial support.

References

1. https://www.bksv.com/en/instruments/daq-data-acquisition/analyzer-system/acoustic-camera-9712
2. https://www.gfaitech.com/products/acoustic-camera
3. https://blogs.sw.siemens.com/simcenter/home-appliances-from-noise-troubleshooting-to-noise-reduction-strategies/
4. S. Oerlemansa, P. Sijtsmaa, and B. Méndez Lópezb, "Location and quantification of noise sources on a wind turbine," Journal of Sound and Vibration, 299(4) 869–883, (2007).
5. F. R. Grosche, H. Stiewitt, and B. Binder. "Acoustic wind-tunnel measurements with a highly directional microphone", AIAA Journal, 15(11), 1590-1596, (1977).
6. W.D. Fonsecaa, S.N.Y Gergesb, and R.P. Dougherty. "Pass-by noise measurements using beamforming technique", 37th International Congress and Exposition on Noise Control Engineering, 26-29 October 2008, Shanghai China.
7. P. Sijtsma. "CLEAN based on spatial source coherence", International Journal of Aeroacoustics, 6(4), 357-374, (2007).
8. T. Padois, J. Fischer, C. J. Doolan, and O. Doutres. "Acoustic imaging with conventional frequency domain beamforming and generalized cross correlation: A comparison study", Applied Acoustics 177, 107914, (2021).
9. J. Olaf. "Strength and weakness of calculating beamforming in the time-domain", Berlin Beamforming Conference (2006).
10. A. Mimani, J. Fischer, D. J. Moreau, and C. J. Doolan. "A comparison of time-reversal and cross-spectral beamforming for localizing experimental rod-airfoil interaction noise sources", Mechanical Systems and Signal Processing, 111, 456-491, (2018).
11. S. Guidati, G. Guidati, and S.Wagner. "Beamforming in a reverberating environment with the use of measured steering vectors", 7th AIAA/CEAS Aeroacoustics Conference, Maastricht, The Netherlands, (2001).
12. B. A. Fenech, and K. Takeda. "Towards more accurate beamforming levels in closed-section wind tunnels via de-reverberation", 13th AIAA/CEAS Aeroacoustics Conference, Italy, Rome, (2007).
13. J. Fischer, and C. Doolan. "Beamforming in a reverberant environment using numerical and experimental steering vector formulations", Mechanical Systems and Signal Processing. 91, 10–22, (2017).
14. P. Sijtsma, and H. Holthusen. "Corrections for mirror sources in phased array processing techniques." 9th AIAA/CEAS Aeroacoustics Conference, Hilton Head.
15. D. Blacodon, and J. Bulte. "Dereverberation of a closed test section of a wind tunnel with a multi microphones cesptral method", The Journal of the Acoustical Society of America 133, 3394 (2013); https://doi.org/10.1121/1.4805894.

16. S. Bousabaa, J. Bulte and D. C. Mincu. “Sparse green’s functions estimation using orthogonal matching pursuit: Application to aeroacoustic beamforming”, AIAA Journal, 56(6), 2252-2270, (2018).
17. J. Fischer, and C. Doolan. “Improving acoustic beamforming maps in a reverberant environment by modifying the cross-correlation matrix”, Journal of Sound and Vibration 411, 129–147, (2017).
18. J. Fischer, and C. Doolan. “An improved eigenvalue background noise reduction method for acoustic beamforming”, Mechanical Systems and Signal Processing 140, 106702, (2020).
19. Z. Prime, and C. Doolan. “A comparison of popular beamforming arrays”, Proceedings of Acoustics, 17th–20th November 2013, Victor Harbor, Australia.
20. T.F. Brooks, and W.M. Humphreys, “A deconvolution approach for the mapping of acoustic sources (DAMAS) determined from phased microphone arrays,” Journal of Sound and Vibration, 294, 856–879, (2006).